Acta Oceanol. Sin., 2023, Vol. 42, No. 5, P. 117–129
https://doi.org/10.1007/s13131-022-2069-2
http://www.aosocean.com
E-mail: ocean2@hyxb.org.cn

Geochemical characteristics of Sr isotopes in the LS33 drill core from the Qiongdongnan Basin, South China Sea, and their response to the uplift of the Tibetan Plateau

Ke Wang[1, 2, 3], Shikui Zhai[1, 3]*, Zenghui Yu[1, 3], Huaijing Zhang[1, 3]

[1] College of Marine Geosciences, Ocean University of China, Qingdao 266100, China

[2] Sinopec Matrix Co., Ltd., Qingdao 266000, China

[3] Key Lab of Submarine Geosciences and Prospecting Techniques, Ministry of Education, Qingdao 266100, China

Received 20 December 2021; accepted 5 July 2022

Abstract

Making full use of modern analytical and testing techniques to explore and establish new indexes or methods for extracting paleoseawater geochemical information from sediments will help to reconstruct the sedimentary paleoenvironment in different research areas. The connection between the subsidence of the South China Sea basin and the uplift of the Tibetan Plateau has been a scientific concern in recent decades. To explore the information on the sedimentary paleoenvironment, provenance changes and uplift of Tibetan Plateau contained in core sediments (debris), we selected core samples from Well LS33 in the Qiongdongnan Basin, South China Sea, and analyzed the contents of typical elements (Al, Th, and rare earth elements) that can indicate changes in provenance and the Sr isotopic compositions, which can reveal the geochemical characteristics of the paleoseawater depending on the type of material (authigenic carbonate and terrigenous detritus). The results show the following: (1) during the late Miocene, the Red River transported a large amount of detrital sediments from the ancient continental block (South China) to the Qiongdongnan Basin. (2) The authigenic carbonates accurately record changes in the $^{87}Sr/^{86}Sr$ ratios in the South China Sea since the Oligocene. These ratios reflect the semi-closed marginal sea environment of the South China Sea (relative to the ocean) and the sedimentary paleoenvironment evolution process of the deep-water area of the Qiongdongnan Basin from continental to transitional and then to bathyal. (3) Since the Neogene, the variations in the $^{87}Sr/^{86}Sr$ ratio in the authigenic carbonates have been consistent with the variations in the uplift rate of the Tibetan Plateau and the sediment accumulation rate in the Qiongdongnan Basin. These consistent changes indicate the complex geological process of the change in the rock weathering intensity and terrigenous Sr flux caused by changes in the uplift rate of the Tibetan Plateau, which influence the Sr isotope composition of seawater.

Key words: sediments from a drill core, grouping analysis, elements and Sr isotopes, provenance and paleoenvironment, uplift of the Tibetan Plateau and subsidence of the South China Sea basin

Citation: Wang Ke, Zhai Shikui, Yu Zenghui, Zhang Huaijing. 2023. Geochemical characteristics of Sr isotopes in the LS33 drill core from the Qiongdongnan Basin, South China Sea, and their response to the uplift of the Tibetan Plateau. Acta Oceanologica Sinica, 42(5): 117–129, doi: 10.1007/s13131-022-2069-2

1 Introduction

Of the natural Sr isotopes, ^{87}Sr is formed from ^{87}Rb by β-decay. Due to the long half-life of ^{87}Rb (approximately 4.9×10^{11} a), only very old continental material has a high $^{87}Sr/^{86}Sr$ ratio originating from ^{87}Rb decay. Terrigenous detritus from the same provenance should have similar $^{87}Sr/^{86}Sr$ ratios, and the obvious change in the $^{87}Sr/^{86}Sr$ ratio of terrigenous detritus in sediments indicates a change in provenance. In the process of weathering, denudation and transport, some elements, such as Al, Th and light rare earth elements (LREEs), often exist in residues and do not easily migrate. Studies have shown that the parent rock properties of the provenance remain the main factor controlling the geochemical composition of the clastic rocks despite the modification of the sedimentary process (Rollinson, 1993). Therefore, the Al and Th contents, LREE/heavy rare earth element (HREE) ratio and $^{87}Sr/^{86}Sr$ ratio in detrital sediments can indicate changes in the input of old terrigenous material.

Sr isotopes generally do not fractionate due to temperature, pressure and microbial effects, and the residence time of Sr in seawater (approximately 2×10^6 a) is much longer than the mixing time of seawater (approximately 1 500 a), so the $^{87}Sr/^{86}Sr$ ratio of ocean water is theoretically uniform at any given time globally (DePaolo, 1986; McArthur et al., 1992). The $^{87}Sr/^{86}Sr$ ratio of carbonate minerals that formed in seawater is the result of a mixture of terrigenous Sr ($^{87}Sr/^{86}Sr$ average: 0.711 9) and mantle-derived Sr ($^{87}Sr/^{86}Sr$ average: 0.703 5) (Palmer and Elderfield, 1985). Therefore, the $^{87}Sr/^{86}Sr$ ratio of marine carbonate minerals can show the input of the two Sr sources to the seawater in the geologic period (Harris, 1995; Zakharov et al., 2018; Bagherpour et al., 2018; Wang et al., 2018). When the $^{87}Sr/^{86}Sr$ curve of marine car-

Foundation item: The National Science and Technology Major Project under contract No. 2011ZX05025-002-03; the Project of China National Offshore Oil Corporation (CNOOC) Limited under contract No. CCL2013ZJFNO729; the National Natural Science Foundation of China under contract No. 41530963.

*Corresponding author, E-mail: zhai2000@ouc.edu.cn

bonate components is compared with the $^{87}Sr/^{86}Sr$ reference curve of ocean water for the same time period, anomalies indicate the occurrence of major regional geological events (Ruppel et al., 1996; Kroeger et al., 2007; Edwards et al., 2015). To recover the Sr isotopic composition of the paleoseawater in the South China Sea, existing studies have been mainly based on the analysis of pure carbonates such as carbonate platform or reef biocarbonate samples. However, in the absence of pure carbonate rocks, it is very difficult to extract paleoseawater geochemical information. Making full use of modern analytical and testing techniques to explore and establish new indexes or methods for extracting geochemical information of paleoseawater from sediments will help to reconstruct the sedimentary paleoenvironment in different research areas.

The regional sedimentary environment of the northwestern South China Sea (Qiongdongnan Basin) has gradually changed from a continental environment to a bathyal environment (Cai et al., 2013; Liu et al., 2015). This process has been occurring since the Oligocene and has coincided with the uplift of the Tibetan Plateau over time, representing a major geological event in Southeast Asia. During the uplift process, the Tibetan Plateau experienced continuous erosion (van der Beek et al., 2009). Many rivers (such as the Red River, Zhujiang River and Mekong River) flowed into the South China Sea and transported large amounts of weathering products from the Tibetan Plateau to the South China Sea. As the South China Sea features a semi-closed environment relative to the open ocean, most of the terrigenous detritus imported into the South China Sea through the abovementioned rivers is trapped in the basin. The sedimentary strata formed by these sediments in different periods must contain information about the uplift of the Tibetan Plateau or record the uplift process of the Tibetan Plateau. Although studies have demonstrated a coupling relationship between the uplift of the Tibetan Plateau and the subsidence of the South China Sea basin based on geochemical records in reef carbonate rocks (Bi et al., 2017), evidence from basin sedimentary records is still lacking. The sediments of the Qiongdongnan Basin in the South China Sea can be divided into two types: authigenic carbonate and terrigenous detritus. The former can be used to extract information on the nature of the paleomarine environment, and the latter can be used to reveal the provenance and changes in it. Based on the analysis of the major and trace elements (including rare earth elements) and Sr isotope compositions of authigenic carbonate and terrigenous detritus in the core samples from Well LS33 (see Fig. 1 for well location) in the Qiongdongnan Basin, combined with research data on the heavy minerals (Liu et al., 2015), particle size composition (Li, 2013) and micropaleontology (Liu et al., 2018) in the core sediments of Well LS33, this paper discusses some important scientific issues, such as the evolution of the chemical properties of paleoseawater and the changes in sediment provenance in the region of Well LS33 since the Oligocene, and further reveals the geochemical response of the Qiongdongnan Basin to the uplift of the Tibetan Plateau.

2 Regional geological characteristics

The Qiongdongnan Basin (17°00′–18°50′N, 108°50′–114°40′E) is located in the northwestern South China Sea, bounded by the Hainan Uplift in the north, Shenhu Uplift in the east, Yongle Uplift in the south and Yinggehai Basin in the west, with an area of over 3×10^4 km^2 (Fig. 1). The main structural pattern of the Qiongdongnan Basin is characterized by north-south zonation and east-west blocks (Tian, 2010; Lei et al., 2011). The north-south zonation means that the basin can be divided into north uplift area, central depression area and south uplift area by the north No. 2 fault zone and south No. 11 fault zone (Fig. 1). The east-west blocks refer to the division of the Qiongdongnan Basin into two rift zones (Fig. 1), with the No. 14 fault zone in the middle of the basin as the boundary. Since the Oligocene, the sedimentary provenance of the Qiongdongnan Basin has been very complicated, and the volcanic activities in the basin, the adjacent uplift zone and the surrounding land have provided sediments to the basin that cannot be ignored. However, the contribution of provenance to the sedimentary filling of the basin is different in different geological periods. To date, nearly 20 scientific or pro-

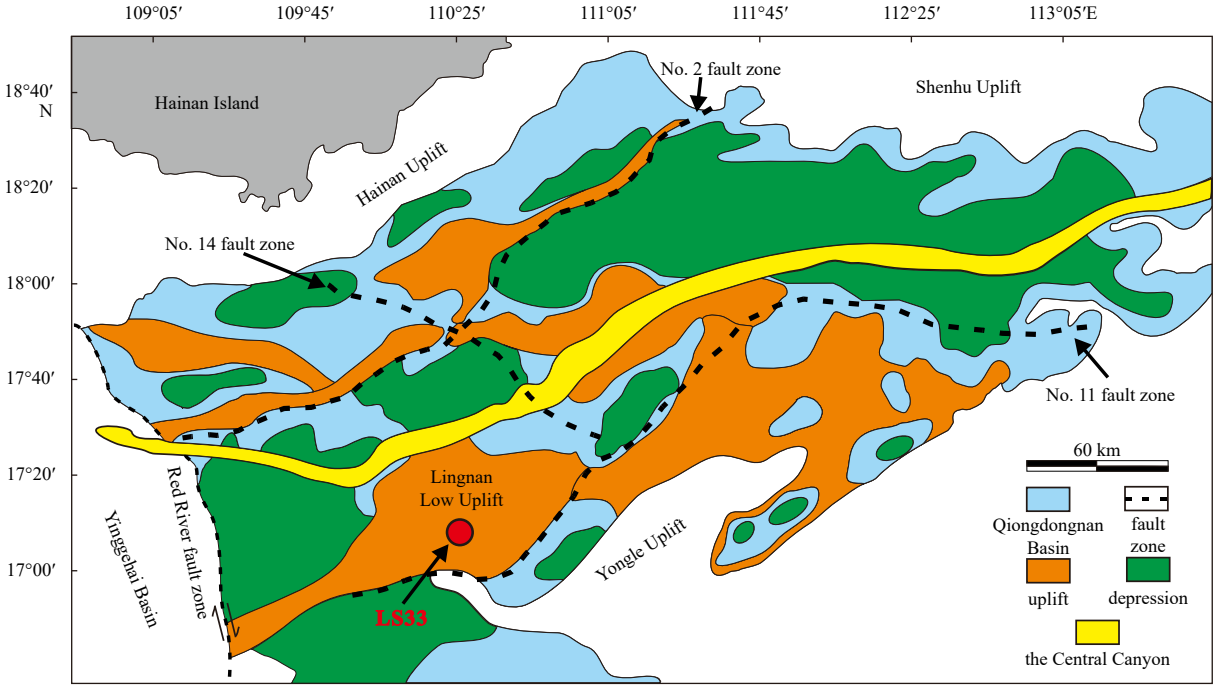

Fig. 1. Topographic map of the Qiongdongnan Basin (modified from Liu et al. (2015)).

duction wells have been drilled in the Qiongdongnan Basin, mainly in the northeast, central and southwest. The research results are mainly in the fields of geophysics, mineralogy, petrology, elemental geochemistry and micropaleontology. For the analysis of provenance evolution in the deep-water area of the Qiongdongnan Basin, there is still a lack of geological evidence based on isotopic geochemistry.

Well LS33 is located in the middle of the Lingnan Low Uplift in the deep-water area of the Qiongdongnan Basin (Fig. 1); the well has a water depth of 1 462.8 m, a drilling completion depth of 4 356 m, and reaches the lower Oligocene Yacheng Formation (Fig. 2). The bottom of Well LS33 is mainly composed of pre-Cenozoic igneous rock, metamorphic rock and sedimentary rock (Wei et al., 2001; Mi et al., 2009; Sun et al., 2011); the bottom overlies a sediment layer with a thickness of more than 2 000 m and that is dominated by Cenozoic sandstone, mudstone and loose sediments. Well LS33 is one of the largest, most continuous, and best-preserved wells in the Qiongdongnan Basin to date. Core sampling has covered continuous sediment formations since the Oligocene, and hence, the LS33 drill core provides the most ideal sample for studying the paleoseawater characteristics of the South China Sea basin, the sedimentary filling history and the relationship with the surrounding major geological events.

3 Samples and analytical methods

3.1 *Core chronostratigraphic framework*

Based on a comprehensive study of the data on seismicity, paleomagnetism and micropaleontological fossils (Liu et al., 2009, 2018; Du, 2013; Chen et al., 2015), the formation boundaries from the lower Pleistocene to the lower Oligocene in Well LS33 (Fig. 2) have been determined, namely, the Quaternary Ledong Formation (2 111–2 214.5 m), Pliocene Yinggehai Formation (2 214.5–2 692 m), upper Miocene Huangliu Formation (2 692–3 152 m), middle Miocene Meishan Formation (3 152–3 373 m), lower Miocene Sanya Formation (3 373–3 672 m), upper Oligocene Lingshui Formation (3 672–3 931 m) and lower Oligocene Yacheng Formation (3 931–4 356 m). The chronostratigraphic framework has been widely used in Qiongdongnan Basin geological research (Chen, 2012; Li et al., 2013; Liu et al., 2015; Bi et al., 2017; Xiu et al., 2018), and its authenticity and accuracy have been fully verified.

3.2 *Core description and sampling*

The Quaternary strata are mainly composed of light gray or gray-green clays intermixed with thin layers of silt or fine sand; these sediments are rich in bioclasts and lack obvious diagenesis. The Pliocene strata are mainly composed of argillaceous and clayey sediments with thin layers of light gray silty or argillaceous sediments. The upper Miocene strata are mainly dark gray mudstone interbedded with thin dark gray siltstone, with foraminifera and fossil fragments and a small amount of glauconite. The middle Miocene strata are mainly dark green-gray to olive-gray calcareous mudstones with carbonate-rich deposits. The upper part of the lower Miocene strata is composed of fine sandstone, siltstone and mudstone, while the lower part is composed of thick massive mudstone with a small amount of thinly bedded argillaceous siltstone. The upper Oligocene strata are mainly olive-gray, dark green-gray, and brown-gray mudstone in the upper part and thick mudstone interbedded with thin limestone in the lower part. The upper part of the lower Oligocene formation is mainly composed of limestone, fine sandstone, argillaceous siltstone and mudstone, while the bottom is characterized by dark green andesite clasts and pyroxene. The lithological changes indicate that the LS33 core is mainly composed of sedimentary rocks or loose sediments, except at the bottom of the lower Oligocene formation. A total of 28 samples were collected for grouping analysis (Fig. 2) and authigenic carbonates were extracted for the analysis of Sr isotopic compositions. The Al_2O_3,

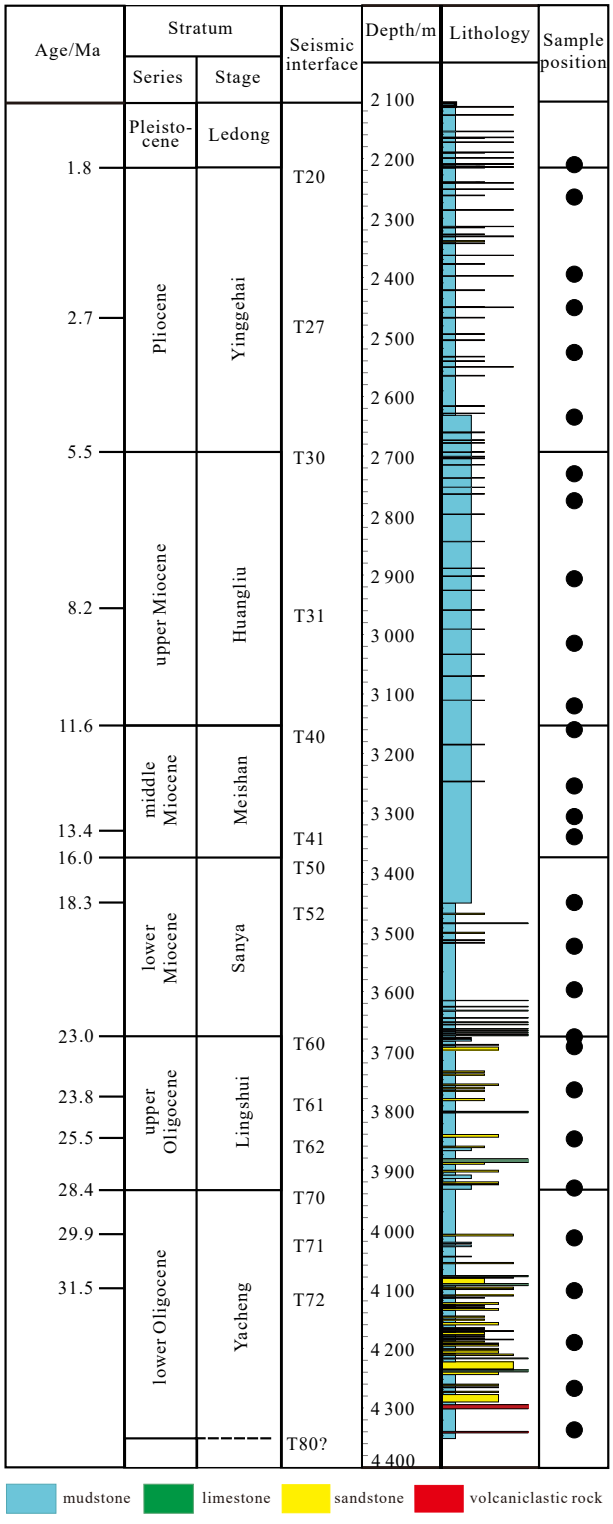

Fig. 2. Lithological profile of Well LS33 (modified from Liu et al. (2018)).

Th, and REE contents and Sr isotopic compositions of terrigenous detritus in the 23 core samples were analyzed.

3.3 *Analytical method*

First, the "organic distillation extraction method" (Chen, 2012) was used to wash oil and pretreat the samples (to remove organic substances, such as lubricating oil, that were mixed in during the drilling process). After oil washing, the samples were dried for 12 h at a constant temperature of 60℃ and ground to below 200 mesh with an agate mortar. The 200 mg sample powder was weighed and placed in a clean Teflon sampler, and HAc (10%) was added. After the carbonate was completely dissolved, the supernatant was centrifuged and used to analyze the authigenic carbonate. Then, 1.5 mL HF, 1.5 mL HNO_3 and 0.2 mL $HClO_4$ were added to the residue and heated on an electric heating plate for 36 h until the sample was completely dissolved. The samples were then steamed until they were nearly dry at 180℃ to remove HF and $HClO_4$ from the solution. Finally, HNO_3 (2%) solution was added for terrigenous detritus analysis. The Sr isotopes were purified by AG50W×12 cation exchange resin (the ratio of HCl to the recycled resin column was 1:1). The sample liquid was added to the exchange column, washed with HCl (2.5 mol/L), received Sr, and then received rare earth elements with HCl (6 mol/L). Finally, the Sr receiver liquid was heated and dried on an electric heating plate. This process was followed for additional purification.

The Al_2O_3 and MnO contents were analyzed by ICP-OES. The Th and REE contents were analyzed by ICP-MS. The reference material was GBW07309. The Sr isotope composition was analyzed by MC-ICP-MS. The reference materials were GBW04411 and NBS987. The detection limits of Al_2O_3, Th and Sr were 24×10^{-6}, 50×10^{-9} and 1×10^{-6}, respectively. The detection limits of the REEs (La–Lu) were 9×10^{-9}, 12×10^{-9}, 6×10^{-9}, 21×10^{-9}, 9×10^{-9}, 6×10^{-9}, 9×10^{-9}, 6×10^{-9}, 6×10^{-9}, 6×10^{-9}, 6×10^{-9}, 3×10^{-9}, respectively. The chemical yield of Sr is the ratio of the sum of Sr contents of each component to the total Sr content of the whole rock, and the values range between 90% and 110%. The samples were pretreated at the Key Lab of Submarine Geosciences and Prospecting Techniques of Ministry of Education (Ocean University of China). The analysis of major and trace elements and Sr isotopes was performed at First Institute of Oceanography, Ministry of Natural Resources.

4 Analytical results

The analytical results of Al_2O_3 and Th contents, LREE/HREE ratios and Sr isotope tests in the LS33 drill core samples are listed in Table 1. The $^{87}Sr/^{86}Sr$ ratios of the terrigenous detritus varied from 0.712 763 1 to 0.720 349 9, with an average value of 0.715 387 7, showing a certain fluctuation range (Table 1, Fig. 3a). During the late Oligocene to middle Miocene (28.4–11.6 Ma), the $^{87}Sr/^{86}Sr$ ratio was relatively low (mean value: 0.713 605 4), indicating that the sediment provenance was relatively stable during this period.

Table 1. $^{87}Sr/^{86}Sr$ ratios of the authigenic carbonate and terrigenous detritus, the Al_2O_3 and Th contents, and LREE/HREE ratios of the terrigenous detritus in the LS33 drill core samples

Chronostratigraphy	Depth/m	$^{87}Sr/^{86}Sr$ ratio (Authigenic carbonate)		Al_2O_3 content/%		Th content/10^{-6}		LREE/HREE ratio		$^{87}Sr/^{86}Sr$ ratio (Terrigenous detritus)	
		Measured value	Mean value	Measured value	Mean value	Measured value	Mean value	Measured value	Mean value	Measured value	Mean value
Quaternary	2 210	0.709 404 0		15.72		14.48		8.83		0.716 263 5	
Pliocene	2 265	0.709 304 2		17.40		14.44		9.27		0.716 865 0	
	2 395	0.709 365 3	0.709 284 3	17.28	17.43	15.18	14.71	9.20	9.12	0.716 392 3	0.716 794 2
	2 450	0.709 413 3		17.35		14.73		9.33		0.717 357 1	
	2 525	0.709 149 9		18.04		14.72		9.11		0.716 676 4	
	2 635	0.709 069 1		18.78		14.68		8.97		0.717 211 1	
Late Miocene	2 730	0.709 053 0		19.27		14.68		9.84		0.720 349 9	
	2 775	0.709 054 8		19.07		15.53		9.58		0.719 497 1	
	2 905	0.709 045 7	0.709 031 4	19.17	19.47	16.27	15.80	9.24	9.50	0.716 178 4	0.717 977 4
	3 015	0.709 011 1		19.52		15.73		9.44		0.716 745 9	
	3 120	0.708 992 4		20.30		16.79		9.39		0.717 115 6	
Middle Miocene	3 160	0.708 988 5		17.94		14.37		8.92		0.714 366 2	
	3 255	0.708 964 8	0.708 944 4	18.18		14.23		7.77		0.713 745 0	
	3 305	0.708 933 0		17.44		14.47		7.43		0.713 747 6	
	3 340	0.708 891 2		17.28		16.25		8.03		0.714 577 1	
Early Miocene	3 451	0.708 774 3		17.14		15.94		7.96		0.713 905 8	
	3 523	0.708 764 7	0.708 750 1	17.00	16.41	17.61	15.11	8.78	8.43	0.713 531 2	0.713 605 4
	3 598	0.708 711 3		17.65		17.67		9.64		0.714 441 6	
Late Oligocene	3 673	0.708 529 8		16.02		13.00		8.11		0.712 878 8	
	3 694	0.708 523 9		16.06		15.11		8.41		0.712 763 1	
	3 766	0.708 458 1	0.708 509 5	15.74		15.47		8.05		0.713 027 0	
	3 847	0.708 548 0		12.90		13.29		8.39		0.713 023 4	
	3 931	0.708 487 5		13.53		13.96		9.72		0.713 258 4	
Early Oligocene	4 015	0.708 489 0		–		–		–		–	
	4 102	0.708 833 7		–		–		–		–	
	4 189	0.708 919 0	0.709 023 8	–	–	–	–	–	–	–	–
	4 267	0.709 243 4		–		–		–		–	
	4 339	0.709 633 8		–		–		–		–	

Note: – represents no data.

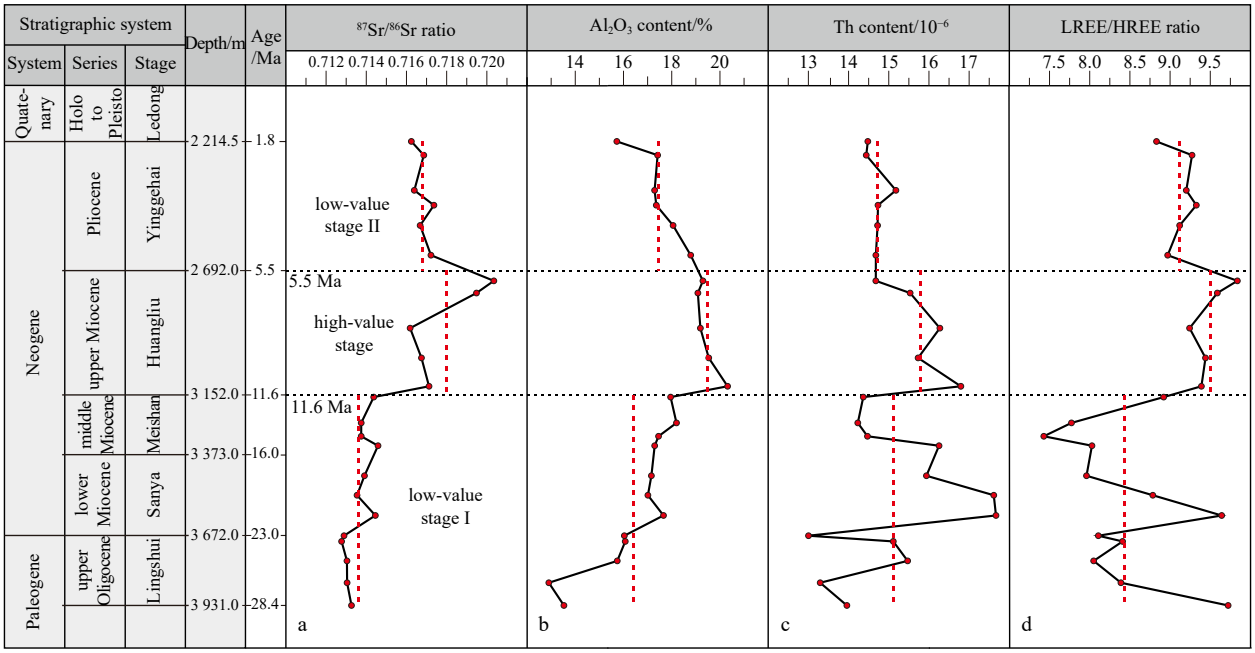

Fig. 3. Comparison curves of the $^{87}Sr/^{86}Sr$ ratios (a), Al_2O_3 contents (b), Th contents (c) and LREE/HREE ratios (d) of the terrigenous detritus in the LS33 drill core samples. The red dotted line represents the average value of each stage.

During the late Miocene (11.6–5.5 Ma), the $^{87}Sr/^{86}Sr$ ratio changed significantly and reached its maximum value (maximum value: 0.720 349 9, average value: 0.717 977 4), indicating that the sedimentary environment or provenance of the study area changed significantly and that relatively old terrigenous sediments entered the Qiongdongnan Basin. In the Pliocene (5.5–1.8 Ma), the $^{87}Sr/^{86}Sr$ ratio (mean value: 0.716 794 2) was relatively stable, but the $^{87}Sr/^{86}Sr$ ratio was higher than that in the stable period from the late Oligocene to middle Miocene, indicating that the change in provenance in the Pliocene tended to be stable again. The trends of the $^{87}Sr/^{86}Sr$ ratios, Al_2O_3 and Th contents, and LREE/HREE ratios of the terrigenous detritus were generally consistent (Fig. 3).

In the Oligocene, the $^{87}Sr/^{86}Sr$ ratio of the authigenic carbonate component gradually decreased from a high value (early Oligocene) to a stable value (late Oligocene) (Fig. 4). Since the Neogene, the $^{87}Sr/^{86}Sr$ ratio of the authigenic carbonate has gradually increased overall, which is consistent with the trend in the $^{87}Sr/^{86}Sr$ ratios of ocean water and reef carbonate rocks of Well Xike-1 in the South China Sea during the same period, but the values of the other two are generally higher than those of ocean water (Fig. 4).

5 Discussion

5.1 *Sr isotopic composition of terrigenous detritus and its provenance implications*

As previously mentioned, the $^{87}Sr/^{86}Sr$ ratios of the terrigenous detritus in core samples have experienced three stages since the late Oligocene (Fig. 3a), namely, low-value stage I (late Oligocene to middle Miocene), high-value stage (late Miocene) and low-value stage II (Pliocene), indicating that there have been three major sedimentary provenance changes in the Qiongdongnan Basin since the late Oligocene.

In low-value stage I (late Oligocene to middle Miocene), the $^{87}Sr/^{86}Sr$ ratio is lower than that in the other two stages, and the average Al_2O_3 and Th contents and average LREE/HREE ratios are also lower in the same period (Fig. 3). During this period, the $^{87}Sr/^{86}Sr$ ratio of the terrigenous detritus generally changes little, indicating that the proportion of ancient terrigenous detritus in the sediments was relatively stable. Compared with the $^{87}Sr/^{86}Sr$ ratio, the Al_2O_3 and Th contents and the LREE/HREE ratio vary greatly, and the latter three should be affected by the mineral composition. This period is a transitional stage from the rifting stage to the postrifting subsidence stage of the basin. The provenance is mainly adjacent highlands, and the mineral composition of the sediments varies greatly (Liu, 2015). The $^{87}Sr/^{86}Sr$ ratio indicates the relative age of the source rock and has little relation with the mineral composition. For example, the $^{87}Sr/^{86}Sr$ ratios in different minerals (such as feldspar, pyroxene and olivine in unmixed mafic magmatic rocks) are similar or consistent.

In the high-value stage (late Miocene), the $^{87}Sr/^{86}Sr$ ratio increased rapidly and even reached a maximum (Fig. 3a). This result indicates that a provenance change occurred during this period, which greatly increased the proportion of ancient terrigenous detritus in the sediments. Previous studies (van Hoang et al., 2009) have shown that a tributary of the Red River (highlighted in red in Fig. 5a) developed and flooded in South China in the late Miocene. The Red River Basin mainly includes the southwestern Yangtze Plate and the western Cathaysia Plate. More importantly, the rocks exposed in the southwestern Yangtze Craton and the western Cathaysia Plate are mainly Triassic and late Paleozoic sedimentary rocks, all of which have relatively high $^{87}Sr/^{86}Sr$ ratios. During this period, a large number of slump deposits developed in the shelf slope break of the Yinggehai Basin between the Qiongdongnan Basin and the mouth of the Red River (Wang et al., 2011b). These slump bodies migrated southward slowly with the help of the topography (high in the north and low in the south) of the Yinggehai Basin and crossed the Ying-Qiong junction into the Qiongdongnan Basin (Fig. 6). Deep canyon turbidity channels across the two basins began to develop (Xie et al., 2006; Yuan et al., 2010; Gong et al., 2011; Su et al., 2014), which

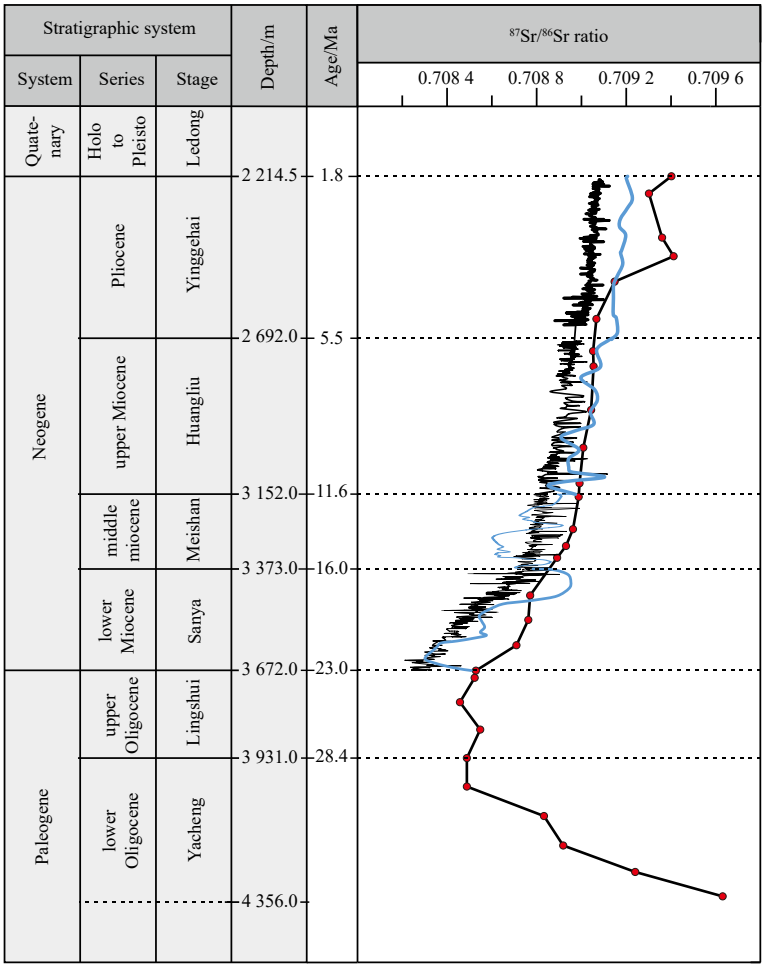

Fig. 4. Comparison curves of the $^{87}Sr/^{86}Sr$ ratios of ocean water (black), reef carbonate of Well Xike-1 (blue) and authigenic carbonate components of Well LS33 core samples (red dot). $^{87}Sr/^{86}Sr$ ratios of reef carbonates in Well Xike-1 are from Bi et al. (2019); $^{87}Sr/^{86}Sr$ ratios of ocean water are from Prokoph et al. (2008).

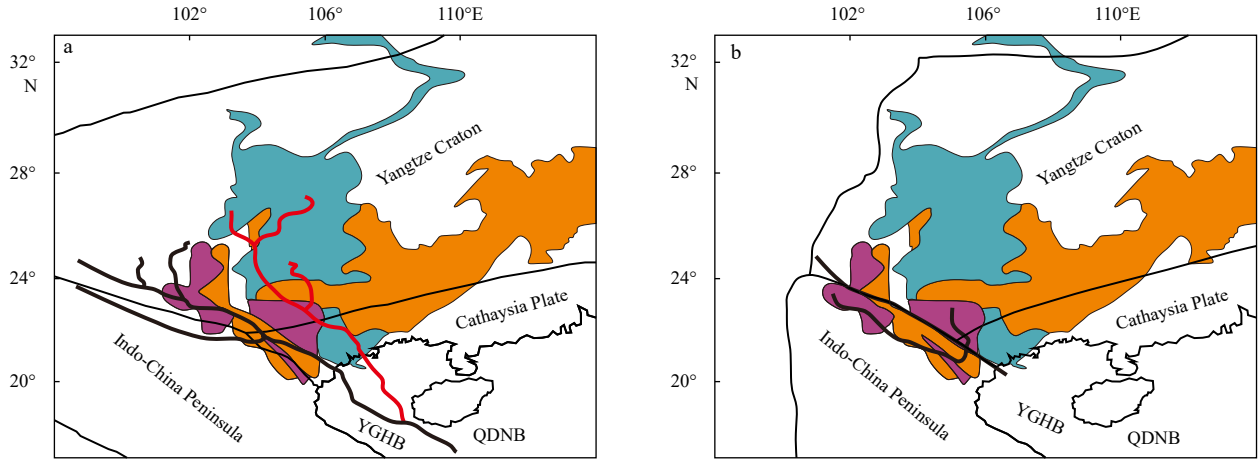

Fig. 5. Changes in the Red River Basin in the late Miocene (a) and modern times (b) (modified from van Hoang et al. (2009)). Orange indicates late Paleozoic sedimentary rocks, blue indicates Triassic sedimentary rocks, and purple indicates early Paleozoic sedimentary rocks. YGHB: Yinggehai Basin; QDNB: Qiongdongnan Basin.

created favorable conditions for the Red River to carry a large amount of terrigenous detritus into the Qiongdongnan Basin. High-resolution seismic profiles show a giant submarine fan that developed in the late Miocene at the junction of the Yinggehai Basin and the Qiongdongnan Basin (Wang et al., 2011b). This submarine fan is connected to the Red River delta by channels (Wang et al., 2011b). Zircon U-Pb ages show that the source of the submarine fan is the Red River Basin (Shao et al., 2019; Xu et

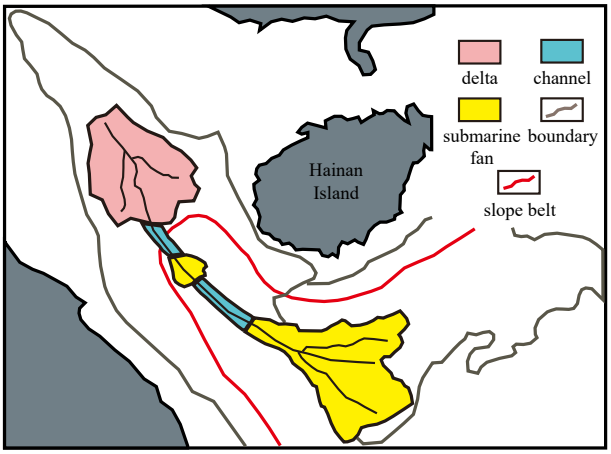

Fig. 6. Schematic diagram of Red River sediment entering the Qiongdongnan Basin in the late Miocene (modified from Wang et al. (2011b)).

al., 2020), thus confirming the existence of a Red River provenance in the western Qiongdongnan Basin from another point of view. In addition, the heavy mineral results also indicate that the sediments from the Red River entered the Qiongdongnan Basin on a large scale in the late Miocene (Liu et al., 2015). Although the current length and basin area of the Red River are not large compared with the surrounding rivers (such as the Changjiang River and the Zhujiang River), its sediment transport to the South China Sea is quite considerable (approximately 130×10^6 t/a; Milliman and Syvitski, 1992). In the late Miocene, the length and basin area of the Red River were much larger than those at present (Fig. 5), and the sediment transport was much larger than that at present. Therefore, the Red River carried a large amount of ancient terrigenous detritus with high $^{87}Sr/^{86}Sr$ ratios from South China into the South China Sea during this period, which may be the main reason for the obvious increase in the $^{87}Sr/^{86}Sr$ ratios. The Al_2O_3 and Th contents and LREE/HREE ratios in the sediments from the same period also show abnormally high values (Fig. 3). On the other hand, these results suggest that more ancient terrigenous detritus entered the Qiongdongnan Basin in the late Miocene.

During the low-value stage II (Pliocene), the $^{87}Sr/^{86}Sr$ ratios decreased rapidly and became stable, indicating that the proportion of ancient terrigenous detritus in the sediments decreased significantly. Under the influence of tectonism, the Red River Basin gradually shrank, and its tributaries gradually shrank to the northern margin of the Indo-China Peninsula (Fig. 5b; van Hoang et al., 2009). As a result, ancient terrigenous detritus from South China was greatly reduced in the basin. In addition, the contribution of Hainan Island to the provenance of the basin increased while the contribution of the Red River provenance decreased (Cao et al., 2013; Liu et al., 2015). The timing of the above geological processes coincides with the rapid decrease in the $^{87}Sr/^{86}Sr$ ratio, indicating that the decrease in the input of ancient terrigenous detritus from South China is the main reason for the rapid decrease in the $^{87}Sr/^{86}Sr$ ratio during this period. The rapid decrease in Al_2O_3 and Th contents and LREE/HREE ratios in sediments during the same period (Fig. 3) also supports this conclusion.

In conclusion, the change in the $^{87}Sr/^{86}Sr$ ratio of the terrigenous detritus reflects the change in the proportion of old terrigenous detritus in the sediments and thus reveals the change in provenance in the Qiongdongnan Basin since the late Oligocene from the perspective of isotope geochemistry. The three stages show the relative variations in Sr input from the ancient continent. The $^{87}Sr/^{86}Sr$ ratio is the highest in the late Miocene, indicating that the stage in which the detrital sediments from the ancient continental block (South China) were numerous extended to the Qiongdongnan Basin. Although the sediments in the Qiongdongnan Basin exhibit the characteristics of multiple heterogenous sources, based on the analysis results of this paper and a large amount of existing research data, the authors suggest that the increase in the $^{87}Sr/^{86}Sr$ ratio in the late Miocene reflects a geological process in which sediments from South China were imported into the western Qiongdongnan Basin (drill location) via the Red River. The vast area of the Red River Basin and the ancient rocks exposed in the basin provided the material basis for the western Qiongdongnan Basin to receive a large number of ancient terrigenous detrital deposits. The deep-water turbidity channel crossing from the Yinggehai Basin into the Qiongdongnan Basin was a transport channel allowing detrital sediments from the Red River to enter the western Qiongdongnan Basin. The Red River submarine fan and its transport channel revealed by the high-resolution seismic profile provide strong evidence for the above viewpoint.

5.2 *Sr isotopic composition of authigenic carbonate and its paleoenvironmental implications*

5.2.1 *Sr isotopic composition of paleoseawater in the South China Sea*

The premise of using carbonate rocks to reconstruct the geochemical characteristics of paleoseawater assumes that the carbonate rocks have not undergone diagenesis and basically retain the original geochemical characteristics present at the time of the rocks' formation. Existing research results (Derry et al., 1989; Kaufman and Knoll, 1995; Le Guerroué et al., 2006) show that authigenic carbonate rocks with Sr contents greater than 200×10^{-6} and Mn/Sr ratios less than 3 are not or are affected only by weak diagenesis, and their Sr isotopic compositions can represent the Sr isotopic compositions of contemporaneous paleoseawater. The Sr contents of authigenic carbonate in the LS33 drill core samples vary from 274.30×10^{-6} to $2\ 130.22\times10^{-6}$ (Table 2) with an average value of $1\ 343.967\times10^{-6}$, which is much higher than 200×10^{-6}, indicating that they are not affected by diagenesis. However, individual samples in the Yacheng Formation (4 339 m, 4 267 m), Yinggehai Formation (2 450 m, 2 395 m, 2 265 m) and Ledong Formation (2 210 m) have high Mn/Sr ratios (greater than 3), which likely indicate that the paleoseawater in the South China Sea was significantly affected by fresh water (fresh water has a higher Mn/Sr ratio). The Mn/Sr ratios of authigenic carbonate in other samples are less than 3 (the Mn/Sr ratio of the sample at a depth of 4 015 m is greater than 3, which needs to be further studied; Table 2) and have no significant correlation with the $^{87}Sr/^{86}Sr$ ratio (Fig. 7), indicating that the $^{87}Sr/^{86}Sr$ ratio is less affected by diagenesis. Therefore, the Sr isotopic compositions of these samples can be used as an indicator of the Sr isotopic composition of the paleoseawater.

Previous studies (Bi et al., 2019) have shown that the variation trend of the $^{87}Sr/^{86}Sr$ ratio of the reef carbonates in Well Xike-1 in the South China Sea can well reflect the trend of the $^{87}Sr/^{86}Sr$ ratio of the coexisting paleoseawater in the South China Sea. As shown in Fig. 8, the variation trend (slowly rising) of the $^{87}Sr/^{86}Sr$ ratio of authigenic carbonates in the LS33 drill core since the Neogene is basically consistent with that of seawater

Table 2. Sr and Mn contents and Mn/Sr ratios of authigenic carbonate in LS33 drill core samples

Chronostratigraphy	Depth/m	Sr content/10^{-6}	Mean value	Mn content/%	Mean value	Mn/Sr ratio
Quaternary	2 210	710.66	710.66	0.37	0.37	5.19
Pliocene	2 265	849.50	1 070.63	0.30	0.28	3.53
	2 395	909.12		0.33		3.62
	2 450	886.74		0.29		3.24
	2 525	1 400.33		0.26		1.89
	2 635	1 307.45		0.22		1.69
Late Miocene	2 730	1 321.12	1 497.18	0.27	0.24	2.01
	2 775	1 372.93		0.20		1.48
	2 905	1 383.49		0.23		1.63
	3 015	1 678.38		0.22		1.29
	3 120	1 729.99		0.27		1.56
Middle Miocene	3 160	1 342.02	1 587.38	0.31	0.32	2.33
	3 255	1 652.94		0.35		2.10
	3 305	1 593.73		0.31		1.92
	3 340	1 760.85		0.30		1.72
Early Miocene	3 451	1 500.05	1 908.61	0.15	0.20	0.97
	3 523	2 095.57		0.24		1.16
	3 598	2 130.22		0.22		1.01
Late Oligocene	3 673	1 536.91	1 335.33	0.13	0.16	0.86
	3 694	1 489.59		0.11		0.73
	3 766	1 486.84		0.15		0.98
	3 847	1 070.38		0.20		1.90
	3 931	1 092.91		0.19		1.75
Early Oligocene	4 015	877.33	1 065.87	0.35	0.40	3.96
	4 102	928.04		0.23		2.44
	4 189	2 914.12		0.52		1.78
	4 267	335.57		0.43		12.92
	4 339	274.30		0.49		18.03

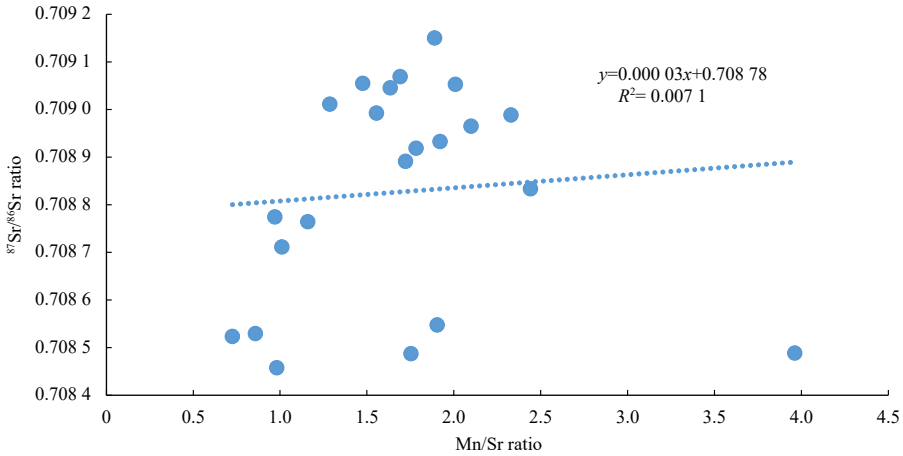

Fig. 7. Covariant diagram of the $^{87}Sr/^{86}Sr$ and Mn/Sr ratios of authigenic carbonate in LS33 drill core samples (4 189–2 525 m).

and the reef carbonates in Well Xike-1 during the same period. This indicates that the authigenic carbonates also effectively record the change in the $^{87}Sr/^{86}Sr$ ratio of the paleoseawater in the South China Sea. However, compared with the $^{87}Sr/^{86}Sr$ ratio of ocean water, the $^{87}Sr/^{86}Sr$ ratios of the authigenic carbonates in Well Xike-1 and Well LS33 are generally higher, which may be related to the semi-closed marginal marine environment of the South China Sea basin. The $^{87}Sr/^{86}Sr$ ratio of the paleoseawater in the South China Sea is affected by the fluxes of terrigenous and mantle-derived Sr. The expansion of the South China Sea was accompanied by a certain scale of volcanic eruptions, resulting in a lower seawater $^{87}Sr/^{86}Sr$ ratio due to the input of mantle-derived Sr. However, the flux of mantle-derived Sr entering the seawater through the seafloor or through surrounding volcanic activity is much smaller than the flux of terrigenous Sr. Even in the global mid-ocean ridge system, where magmatic eruption and hydrothermal activity are the most intense, the flux of mantle-derived Sr to the sea is only about 1/3 of that of terrestrial Sr (Palmer and Edmond, 1989). Therefore, the change in the $^{87}Sr/^{86}Sr$ ratio in the South China Sea since the Neogene has mainly been controlled by the change in the flux of terrigenous Sr. The land surrounding the South China Sea includes many large rivers such as the Red

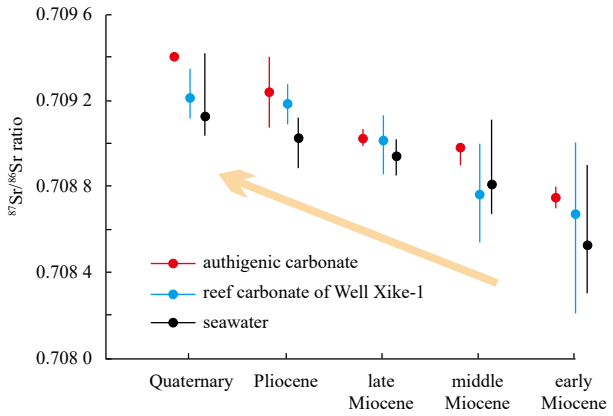

Fig. 8. $^{87}Sr/^{86}Sr$ ratio (dots represent average values and line segments represent the range of variation) of authigenic carbonates (red), reef carbonates in Well Xike-1, seawater of the South China Sea (blue; Bi et al., 2019) and the ocean (black; Prokoph et al., 2008).

River, the Mekong River and the Zhujiang River, which transport large amounts of terrigenous Sr to the sea. Surrounded by the Indo-China Peninsula, South China Mainland and a series of islands, the South China Sea is only connected with the ocean through channels or waterways. The paleoseawater therefore mixed unevenly with ocean water, resulting in a large amount of terrigenous Sr enrichment in the South China Sea. Therefore, the authigenic carbonates of the Well LS33 and the reef carbonates of Well Xike-1 located in different regions of the South China Sea have higher $^{87}Sr/^{86}Sr$ ratios than the ocean water of the same period.

A comparison of Figs 3a and 4 shows that the $^{87}Sr/^{86}Sr$ ratio curves of authigenic carbonate and terrigenous detritus are quite different. First, the $^{87}Sr/^{86}Sr$ ratio of the authigenic carbonate component (maximum value: 0.709 413 3; Table 1) is significantly lower than the $^{87}Sr/^{86}Sr$ ratio of the terrigenous detritus (minimum value: 0.712 763 1; Table 1). Second, the variation in the $^{87}Sr/^{86}Sr$ ratio of the authigenic carbonate since the Neogene is consistent with that of contemporaneous ocean water (increasing slowly) but obviously different from that of the terrigenous detritus (in the three stages). The completely different characteristics of the curve further indicate that the $^{87}Sr/^{86}Sr$ ratio of the authigenic carbonate component in the LS33 drill core can adequately reveal the variation in the Sr isotope composition of the ancient seawater in the South China Sea.

5.2.2 *Sedimentary paleoenvironment*

The sediments deposited in the early Oligocene in Well LS33 did not contain glauconite or other marine minerals. Subsequently, glauconite and other marine minerals began to appear, indicating that the sedimentary environment in the study area changed from continental to a transitional environment. The clay content in the sediments of the Yacheng Formation gradually increased from a low value (Fig. 9), indicating that the hydrodynamic conditions in the early Oligocene changed from strong to weak. The contents of dolomite and pyrite in the core sediments during this period fluctuated (Fig. 9), reflecting the fluctuation in water depth, but the content of terrigenous heavy mineral continued to decrease. In addition, benthic foraminifera were very rare in the bottom sediments of the Yacheng Formation, and their content began to increase in the middle and upper part of the Yacheng Formation (Liu et al., 2018). The above facts indicate that during the early Oligocene, the sedimentary environment in the study area changed from a continental environment to a transitional and neritic environment. In the early

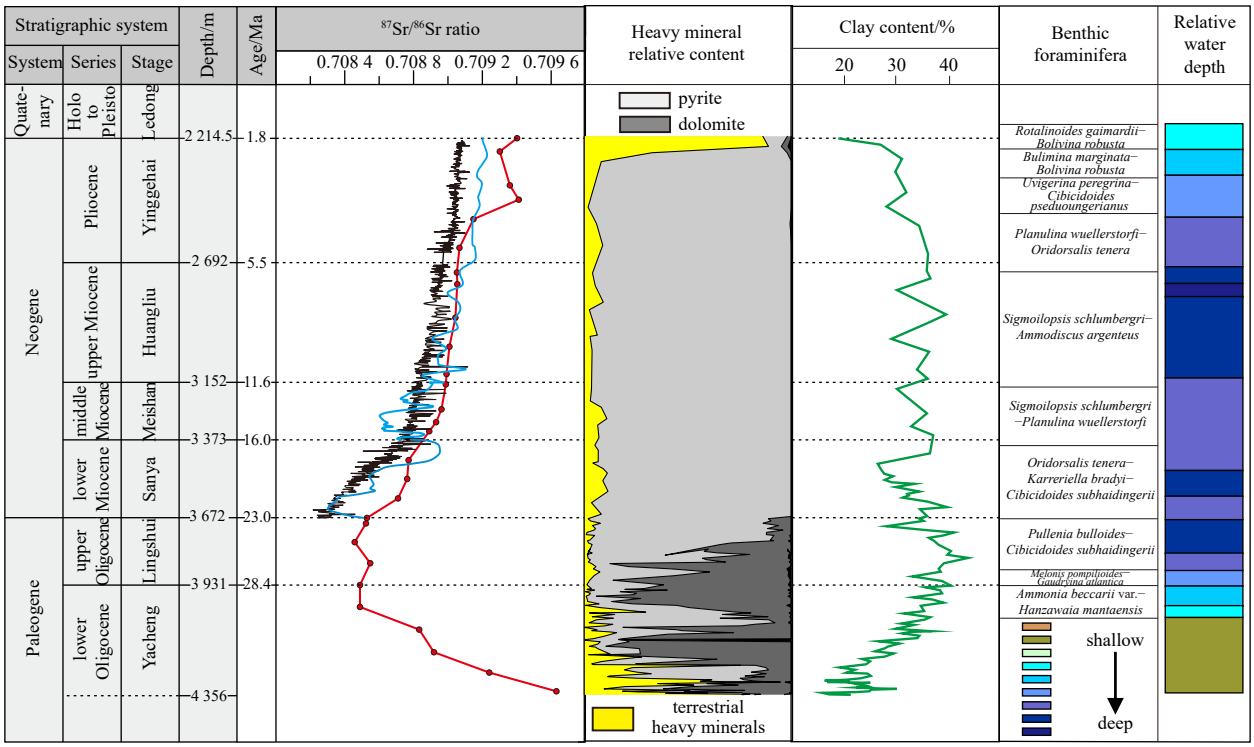

Fig. 9. $^{87}Sr/^{86}Sr$ ratio of authigenic carbonates, heavy mineral composition (Liu et al., 2015), clay content (Li, 2013), and benthic foraminifer assemblage (Liu et al., 2018) in the LS33 drill core.

Oligocene, the $^{87}Sr/^{86}Sr$ ratio of authigenic carbonates experienced a gradual decrease from a high value with very large variations (Fig. 9). In the early continental and transitional environments, the authigenic carbonates mainly formed from river water (or seawater greatly influenced by river water), and the river water had a high $^{87}Sr/^{86}Sr$ ratio due to the terrigenous Sr influence. Therefore, the authigenic carbonates had high $^{87}Sr/^{86}Sr$ ratios in the early Oligocene. As the sedimentary environment gradually changed to the neritic environment, the composition of the water that formed authigenic carbonates gradually approached that of seawater, and the seawater had a lower $^{87}Sr/^{86}Sr$ ratio than the river water. Therefore, the $^{87}Sr/^{86}Sr$ ratio of the authigenic carbonates continued to decrease in the middle and late early Oligocene (Fig. 9).

The particle size of the sediments in the Lingshui Formation was significantly smaller than that in the Yacheng Formation (Fig. 9), indicating that the hydrodynamic conditions in the study area during this period were weak. Benthic foraminifera in sediments during this period were more abundant and distributed continuously, with dominant species gradually evolving from offshore to neritopelagic species (Liu et al., 2018). With the change in the sedimentary environment, the content of authigenic pyrite formed in a deepwater anoxic environment also increased significantly (Fig. 9). The above facts indicate that in the late Oligocene, the water depth in the study area increased further, and the sedimentary environment basically changed into a stable neritic environment. At this time, the composition of the water that formed the authigenic carbonates was close to that of seawater, and the effect of terrigenous Sr on the Sr isotopic composition of seawater gradually decreased. Therefore, the $^{87}Sr/^{86}Sr$ ratios of the authigenic carbonates were relatively stable (Fig. 9).

The particle size of the sediments in the Sanya Formation was relatively coarse due to the influence of the Baiyun Movement at the end of Oligocene (Li, 2013; Fig. 9). Subsequently, the clay content increased, indicating that the hydrodynamic conditions changed from strong to weak. During the middle and late Miocene, the clay content of the core sediments was always high (Fig. 9), indicating that the hydrodynamic conditions were always weak during this period. During the Miocene, dolomite almost disappeared from the core sediments, while authigenic pyrite content was extremely high (Fig. 9), indicating that the study area was in a stable bathyal environment during this period. In addition, benthic foraminifera in the sediments of Sanya and Meishan formations were dominated by bathyal species (Liu et al., 2018), indicating that the study area was in a bathyal environment. The benthic foraminifera in the sediments of the Huangliu Formation were mainly abyssal species (Liu et al., 2018), indicating that the study area was once in a deep-sea environment with a great water depth. The above facts indicate that in the Miocene the water depth of the study area changed to some extent, but it was basically in the neritic to bathyal environment. The slow increase in the $^{87}Sr/^{86}Sr$ ratio of the authigenic carbonates in this period (Fig. 9) reflected the stable bathyal environment in the study area.

The clay content in the bottom sediments from the Yinggehai Formation to the Ledong Formation decreased significantly (Fig. 9), indicating that the hydrodynamic conditions became stronger during this period. From the late Pliocene to the early Quaternary, the proportion of terrigenous heavy minerals increased significantly (Fig. 9), indicating that the basin received a large amount of terrigenous sediments during this period. The benthic foraminifera in the sediments of the Yinggehai Formation were mainly bathyal, and neritic species appeared at the bottom of the Ledong Formation (Liu et al., 2018), reflecting that the water depth in the study area gradually became shallower. The above facts indicate that from Pliocene to early Quaternary, the water depth in the study area became shallower and more terrigenous sediments entered the basin. Therefore, the obvious increase in the $^{87}Sr/^{86}Sr$ ratio of the authigenic carbonates in this period (Fig. 9) reflected the greater input of terrigenous Sr into the seawater.

5.3 *Coupling relationship among the $^{87}Sr/^{86}Sr$ ratio of authigenic carbonates, uplift of the Tibetan Plateau and subsidence of the South China Sea basin*

The uplift of the Tibetan Plateau is the result of the collision between the Indian and Eurasian plates. As early as the 1990s, it was recognized that the uplift of the Tibetan Plateau could be divided into different stages (Li, 1995). Zhong and Ding (1996), based on the fission track dating data of apatite, proposed that the uplift of the Tibetan Plateau had multiple stages (45–38 Ma, 25–17 Ma, 13–8 Ma, and 3 Ma to present) and an uneven velocity, among which the uplift at 3 Ma was the most intense. Luo et al. (2006) traced the formation and evolutionary history of the Tibetan Plateau based on the study of Cenozoic mantle-derived magmatic activities on the Tibetan Plateau and believed that approximately 45 Ma, 27 Ma and 4 Ma were three important evolutionary time nodes, and approximately 45 Ma was the initiation time of the plateau formation. The plateau was formed at approximately 27 Ma, and the maximum uplift speed and amplitude of the Tibetan Plateau occurred at 4 Ma. Wang et al. (2011a) systematically summarized and studied the cryogenic thermochronology records, sedimentary records and tectonic deformation records of Cenozoic strata in different areas of the Tibetan Plateau and suggested four major tectonic uplift and exhumation stages, namely, 60–35 Ma, 25–17 Ma, 12–8 Ma (18–13 Ma in southern Tibet) and approximately 5 Ma to present, among which 18–13 Ma and 5 Ma all show rapid uplift. Thus, the multistage uplift model of the Tibetan Plateau has been widely accepted. Recently, Jiang and Li (2014) proposed a new model of episodic uplift of the Tibetan Plateau based on an analysis of high-resolution seismic profile and borehole data in the southern Tarim Basin, for which the uplift rates of the Tibetan Plateau in different stages of geological history can be calculated. This result provides valuable data for studying the uplift history of the Tibetan Plateau since the Neogene.

As an important global geological event in the late Cenozoic and the most active tectonic movement in Southeast Asia since the Neogene, the uplift of the Tibetan Plateau has greatly affected the sediment supply of the surrounding ocean basins. The South China Sea is adjacent to the Tibetan Plateau and connected to it by three rivers (the Red River, Zhujiang River and Mekong River). The uplift of the Tibetan Plateau greatly influences the sedimentary filling of the South China Sea basin. The formation of thick Quaternary sediments in the Yinggehai Basin located at the mouth of the Red River is the result of the eastward extension of the uplifted area of the Tibetan Plateau, resulting in large amounts of sediments flowing into the sea (Wang, 1995). Previous studies (Sun et al., 1997; Bi et al., 2017, 2019) have shown that the Xisha Islands located in the southeastern Yinggehai Basin were also affected by the uplift of the Tibetan Plateau during their formation process, and the uplift rate of the Tibetan Plateau since the Neogene showed a very consistent trend with the growth rate of the reefs and the rate of increase in the $^{87}Sr/^{86}Sr$ ratio of the reef carbonate rocks.

Figure 10b shows that the change in the Tibetan Plateau uplift rate has four obvious stages, namely, rapid uplift stage I (early Miocene), slow uplift stage (middle Miocene, uplift rate de-

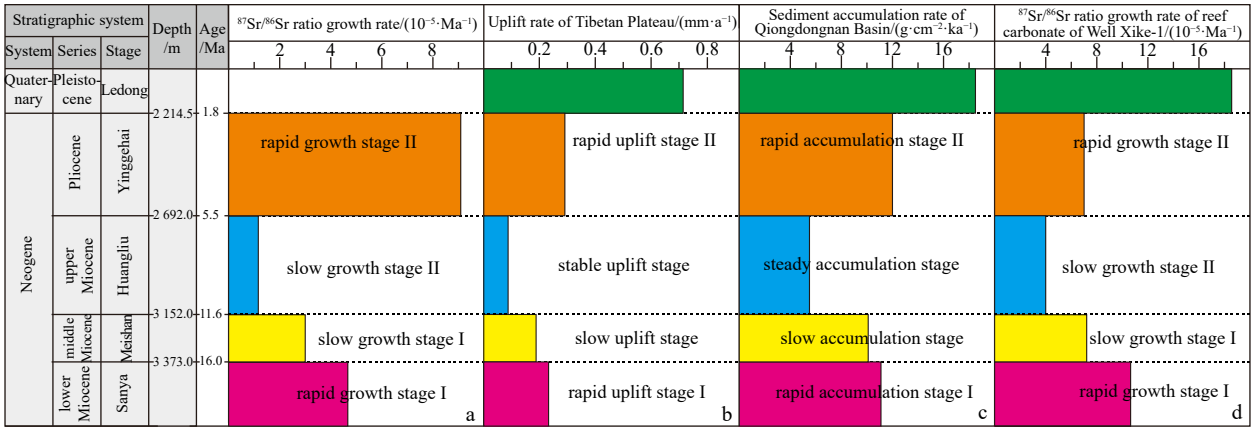

Fig. 10. Comparison curves of $^{87}Sr/^{86}Sr$ ratio growth rate of authigenic carbonate in Well LS33 (a), uplift rate of the Tibetan Plateau (b), sediment accumulation rate in Qiongdongnan Basin (c), and the $^{87}Sr/^{86}Sr$ ratio of the reef carbonates in Well Xike-1 (d) (the data in b are from Jiang and Li (2014); the data in c are from Huang and Wang (2006); the data in d are from Bi et al. (2019)).

creases), stable uplift stage (late Miocene, uplift rate is at a minimum) and rapid uplift stage II (since the Pliocene, uplift rate increases rapidly). The Qiongdongnan Basin sediment accumulation rate (Fig. 10c) is also similar to the trend of the former, namely, rapid accumulation stage I (early Miocene), slow accumulation stage (middle Miocene, accumulation rate decreases), steady accumulation stage (late Miocene, accumulation rate is at a minimum) and rapid accumulation stage II (since the Pliocene, accumulation rate increases rapidly). Sedimentary filling and tectonic subsidence are usually synchronous in basins. Sediment supply and tectonic subsidence are the most important factors controlling sedimentary accumulation. On the one hand, the weathering products formed by the uplift of the Tibetan Plateau directly or indirectly provided sufficient sediments to the basin. On the other hand, the expansion and subsidence of the South China Sea basin provided the accommodation in the basin. The full collision between the Indian and Eurasian plates occurred in the Eocene–Oligocene (Xu et al., 2011) and the Tibetan Plateau began to uplift. The strong collision caused the Indo-China Block to escape southward relative to the South China Block. Thus, the Red River fault zone was formed (Briais et al., 1993). This large fault zone divided the South China Sea and its surrounding areas into two completely different regions with different structural styles and dynamic deformation mechanisms (Lei et al., 2015), namely, the extrusion escape zone to the west of the fault zone (where the Yinggehai Basin was located) and the subduction drag zone (where the Qiongdongnan Basin was located) to the east of the fault zone. The subduction drag zone was mainly controlled by the subduction of the ancient South China Sea under Borneo (Hutchison, 1989; Holloway, 1982). The southward subduction of the South China Sea resulted in the stretching and thinning of the South China continental margin and the formation of a series of fault basins, including the Qiongdongnan Basin. Therefore, the present tectonic pattern of the Tibetan Plateau and the South China Sea basin was formed by the collision of the Indian and Eurasian plates and the subduction of the ancient South China Sea. The good correspondence between the uplift rate of the Tibetan Plateau and the sediment accumulation rate in the Qiongdongnan Basin is a macroscopic reflection of lithospheric plate movement, which is driven by the deeper mantle. The driving mechanism must be explored from the perspective of internal dynamics and tectonics of the Earth, and further studies are needed.

The rate of increase in the $^{87}Sr/^{86}Sr$ ratio of the authigenic carbonates in Well LS33 (Fig. 10a) and that of the reef carbonates in Well Xike-1 (Fig. 10d) also showed a trend consistent with the above two trends, namely, rapid growth stage I (early Miocene), slow growth stage I (middle Miocene, gradual decrease in the growth rate), slow growth stage II (late Miocene with the lowest growth rate) and rapid growth stage II (since the Pliocene, rapid increase in the growth rate). First, the uplift of the Tibetan Plateau caused mechanical extrusion, an expansion of the weathering area and an increase in the surface of the slope, which has greatly increased the strength of the rock weathering in the Tibetan Plateau and its surrounding areas and the efficiency of the fluvial transport of terrigenous sediment to the sea. These processes have led to an increase in the flux of terrigenous Sr and the $^{87}Sr/^{86}Sr$ ratio of seawater. The consistent change in the rate of change in $^{87}Sr/^{86}Sr$ ratios of authigenic carbonates and the uplift rate of the Tibetan Plateau is the concrete embodiment of this geological process. In addition, the South China Sea is a semi-closed marginal sea connected with the western Pacific through waterways. The mixing of seawater in the South China Sea and Pacific is limited to a certain extent. The geochemical characteristics of the seawater in the South China Sea are more significantly affected by the input of terrigenous materials than those of ocean water.

6 Conclusions

The changes in the $^{87}Sr/^{86}Sr$ ratio of the terrigenous detritus from Well LS33 record the change in sediment provenance in the Qiongdongnan Basin since the late Oligocene, which can be clearly divided into three stages (low-value stage I of the late Oligocene to middle Miocene, high-value stage of the late Miocene and low-value stage II of the Pliocene), among which the late Miocene was the peak period when detrital sediments from the ancient continental block (South China) entered the Qiongdongnan Basin.

The authigenic carbonates can accurately record the changes in the $^{87}Sr/^{86}Sr$ ratios in the South China Sea since the Oligocene. The $^{87}Sr/^{86}Sr$ ratio in the South China Sea is generally higher than that in global ocean water, which is a reflection of the influence of the Tibetan Plateau uplift on the South China Sea and (relative to the ocean) the semi-closed marginal sea environment of the South China Sea.

Combined with particle size, heavy mineral and micropale-

ontological data, the Sr isotopic compositions of authigenic carbonates can clearly reveal the evolution of the sedimentary paleoenvironment in the deep-water area of the Qiongdongnan Basin since the Oligocene. During the early Oligocene, the sedimentary environment of the basin changed from continental and transitional to neritic. In the late Oligocene, the basin was basically in a marine sedimentary environment dominated by littoral and neritic environments. In the Miocene, the basin developed a bathyal environment. In the Pliocene to early Quaternary, the basin developed a neritic environment.

Since the Neogene, the variation in the $^{87}Sr/^{86}Sr$ ratio of the authigenic carbonates has been consistent with the variation in the uplift rate of the Tibetan Plateau and the sedimentary accumulation rate in the Qiongdongnan Basin. This consistency indicates a complex geological process involving changes in the rock weathering intensity and terrigenous Sr flux caused by changes in the uplift rate of the Tibetan Plateau, which influences the Sr isotopic composition of seawater.

Acknowledgements

The authors would thank Xiaofeng Liu, Dongjie Bi and Xia Zhang for their help concerning improvement to this article.

References

Bagherpour B, Bucher H, Schneebeli-Hermann E, et al. 2018. Early Late Permian coupled carbon and strontium isotope chemostratigraphy from South China: Extended Emeishan volcanism?. Gondwana Research, 58: 58–70, doi: 10.1016/j.gr.2018.01.011

Bi Dongjie, Zhang Daojun, Zhai Shikui, et al. 2017. The coupling relationships among the Qinghai-Tibet Plateau uplifting, the Qiongdongnan Basin subsiding and the Xisha Islands' Reefs developing. Haiyang Xuebao (in Chinese), 39(1): 52–63

Bi Dongjie, Zhang Daojun, Zhai Shikui, et al. 2019. Seawater $^{87}Sr/^{86}Sr$ values recorded by reef carbonates from the Xisha Islands (South China Sea) since the Neogene and its response to the uplift of Qinghai-Tibetan Plateau. Geological Journal, 54(6): 3878–3890, doi: 10.1002/gj.3386

Briais A, Patriat P, Tapponnier P. 1993. Updated interpretation of magnetic anomalies and seafloor spreading stages in the South China Sea: Implications for the Tertiary tectonics of Southeast Asia. Journal of Geophysical Research: Solid Earth, 98(B4): 6299–6328, doi: 10.1029/92JB02280

Cai Guofu, Shao Lei, Qiao Peijun, et al. 2013. Marine transgression and evolution of depositional environment in the Paleogene strata of Qiongdongnan Basin, South China Sea. Acta Petrolei Sinica (in Chinese), 34(S2): 91–101

Cao Licheng, Jiang Tao, Wang Zhenfeng, et al. 2013. Characteristics of heavy minerals and their implications for Neogene provenances evolution in Qiongdongnan Basin. Journal of Central South University (Science and Technology) (in Chinese), 44(5): 1971–1981

Chen Kui. 2012. Sediment source analysis of oil and gas objective strata in the Qiongdongnan Basin (in Chinese) [dissertation]. Qingdao: Ocean University of China

Chen Hongyan, Sun Zhipeng, Zhai Shikui, et al. 2015. Analysis of well-seismic stratigraphic correlation and establishment of regional stratigraphic framework in the Qiongdongnan Basin of northern South China Sea. Haiyang Xuebao (in Chinese), 37(5): 1–14

DePaolo D J. 1986. Detailed record of the Neogene Sr isotopic evolution of seawater from DSDP Site 590B. Geology, 14(2): 103–106, doi: 10.1130/0091-7613(1986)14<103:DROTNS>2.0.CO;2

Derry L A, Keto L S, Jacobsen S B, et al. 1989. Sr isotopic variations in Upper Proterozoic carbonates from Svalbard and East Greenland. Geochimica et Cosmochimica Acta, 53(9): 2331–2339, doi: 10.1016/0016-7037(89)90355-4

Du Tongjun. 2013. Sequence stratigraphic and deep water sedimentary characteristic in the Qiongdongnan Basin (in Chinese) [dissertation]. Qingdao: Ocean University of China

Edwards C T, Saltzman M R, Leslie S A, et al. 2015. Strontium isotope ($^{87}Sr/^{86}Sr$) stratigraphy of Ordovician bulk carbonate: Implications for preservation of primary seawater values. Geological Society of America Bulletin, 127(9–10): 1275–1289

Gong Chenglin, Wang Yingmin, Zhu Weilin, et al. 2011. The Central Submarine Canyon in the Qiongdongnan Basin, northwestern South China Sea: Architecture, sequence stratigraphy, and depositional processes. Marine and Petroleum Geology, 28(9): 1690–1702, doi: 10.1016/j.marpetgeo.2011.06.005

Harris N. 1995. Significance of weathering Himalayan metasedimentary rocks and leucogranites for the Sr isotope evolution of seawater during the early Miocene. Geology, 23(9): 795–798, doi: 10.1130/0091-7613(1995)023<0795:SOWHMR>2.3.CO;2

Holloway N H. 1982. North Palawan block, Philippines-its relation to Asian mainland and role in evolution of South China Sea. American Association of Petroleum Geologists Bulletin, 66(9): 1355–1383

Huang Wei, Wang Pinxian. 2006. Sediment mass and distribution in the South China Sea since the Oligocene. Science in China Series D: Earth Sciences, 49(11): 1147–1155, doi: 10.1007/s11430-006-2019-4

Hutchison C. 1989. Geological Evolution of Southeast Asia. Oxford: Clarendon Press

Jiang Xiaodian, Li Zhengxiang. 2014. Seismic reflection data support episodic and simultaneous growth of the Tibetan Plateau since 25 Myr. Nature Communications, 5: 5453, doi: 10.1038/ncomms6453

Kaufman A J, Knoll A H. 1995. Neoproterozoic variations in the C-isotopic composition of seawater: Stratigraphic and biogeochemical implications. Precambrian Research, 73(1–4): 27–49

Kroeger K F, Reuter M, Forst M H, et al. 2007. Eustasy and sea water Sr composition: application to high-resolution Sr-isotope stratigraphy of Miocene shallow-water carbonates. Sedimentology, 54(3): 565–585, doi: 10.1111/j.1365-3091.2006.00849.x

Le Guerroué E, Allen P A, Cozzi A. 2006. Chemostratigraphic and sedimentological framework of the largest negative carbon isotopic excursion in Earth history: The Neoproterozoic Shuram formation (Nafun Group, Oman). Precambrian Research, 146(1–2): 68–92

Lei Chao, Ren Jianye, Pei Jianxiang, et al. 2011. Tectonic framework and multiple episode tectonic evolution in deepwater area of Qiongdongnan Basin, northern continental margin of South China Sea. Earth Science-Journal of China University of Geosciences (in Chinese), 36(1): 151–162

Lei Chao, Ren Jianye, Zhang Jing. 2015. Tectonic province divisions in the South China Sea: implications for basin geodynamics. Earth Science-Journal of China University of Geosciences (in Chinese), 40(4): 744–762, doi: 10.3799/dqkx.2015.062

Li Tingdong. 1995. The uplifting process and mechanism of the Qinhai-Tibet Plateau. Acta Geoscientia Sinica (in Chinese), 16(1): 1–9

Li Na. 2013. The sedimentary paleoenvironment and provenance analysis in deepwater area of Qiongdongnan Basin since Oligocene (in Chinese) [dissertation]. Qingdao: Ocean University of China

Liu Xiaofeng. 2015. The evolution of sedimentary paleoenvironment and provenance in the deepwater area of the Qiongdongnan Basin (in Chinese) [Dissertation]. Qingdao: Ocean University of China

Liu Xiaofeng, Sun Zhipeng, Liu Xinyu, et al. 2018. Chronostratigraphic framework based on micro-paleontological data from drilling LS33a in deep water area of northern South China Sea. Acta Sedimentologica Sinica (in Chinese), 36(5): 890–902

Liu Xinyu, Xie Jinyou, Zhang Huolan, et al. 2009. Chronostratigraphy of planktonic foraminifera in the Yinggehai-Qiongdongnan Basin. Acta Micropalaeontologica Sinica (in Chinese), 26(2): 181–192

Liu Xiaofeng, Zhang Daojun, Zhai Shikui, et al. 2015. A heavy mineral viewpoint on sediment provenance and environment in the

Qiongdongnan Basin. Acta Oceanologica Sinica, 34(4): 41–55, doi: 10.1007/s13131-015-0648-1

Luo Zhaohua, Mo Xuanxue, Hou Zengqian, et al. 2006. An integrated model for the Cenozoic evolution of the Tibetan Plateau: constraints from igneous rocks. Earth Science Frontiers (in Chinese), 13(4): 196–211

McArthur J M, Burnett J, Hancock J M. 1992. Strontium isotopes at K/T boundary. Nature, 355(6355): 28, doi: 10.1038/355028a0

Mi Lijun, Yuan Yusong, Zhang Gongcheng, et al. 2009. Characteristics and genesis of geothermal field in deep-water area of the northern South China Sea. Acta Petrolei Sinica (in Chinese), 30(1): 27–32

Milliman J D, Syvitski J P M. 1992. Geomorphic/tectonic control of sediment discharge to the ocean: The importance of small mountainous rivers. The Journal of Geology, 100(5): 525–544, doi: 10.1086/629606

Palmer M R, Edmond J M. 1989. The strontium isotope budget of the modern ocean. Earth & Planetary Science Letters, 92(1): 11–26

Palmer M R, Elderfield H. 1985. Sr isotope composition of sea water over the past 75 Myr. Nature, 314(6011): 526–528, doi: 10.1038/314526a0

Prokoph A, Shields G A, Veizer J. 2008. Compilation and time-series analysis of a marine carbonate $\delta^{18}O$, $\delta^{13}C$, $^{87}Sr/^{86}Sr$ and $\delta^{34}S$ database through Earth history. Earth-Science Reviews, 87 (3–4): 113–133

Rollinson H R. 1993. Using Geochemical Data: Evaluation, Presentation, Interpretation. New York: Longman Scientific Technical, 48–51

Ruppel S C, James E W, Barrick J E, et al. 1996. High-resolution $^{87}Sr/^{86}Sr$ chemostratigraphy of the Silurian: Implications for event correlation and strontium flux. Geology, 24(9): 831–834, doi: 10.1130/0091-7613(1996)024<0831:HRSSCO>2.3.CO;2

Shao Lei, Cui Yuchi, Qiao Peijun, et al. 2019. Implications on the Early Cenozoic palaeogeographical reconstruction of SE Eurasian margin based on northern South China Sea palaeo-drainage system evolution. Journal of Palaeogeography (in Chinese), 21(2): 216–231

Su Ming, Xie Xinong, Xie Yuhong, et al. 2014. The segmentations and the significances of the Central Canyon System in the Qiongdongnan Basin, northern South China Sea. Journal of Asian Earth Sciences, 79: 552–563, doi: 10.1016/j.jseaes.2012.12.038

Sun Zhiguo, Han Changfu, Ju Lianjun, et al. 1997. Comparison between the uplift of the Tibetan Plateau and the sedimentation of coral reefs in Xisha Islands. Marine Sciences (in Chinese), 24(4): 64–67

Sun Zhuan, Liu Hao, Wu Zhe. 2011. The analysis of Cenozoic tectonic sequence of Qiongdongnan Basin in the South China Sea. Offshore Oil (in Chinese), 31(1): 8–15

Tian Shanshan. 2010. Tectonic subsidence analysis and paleotopography restoration of postrifting strata in the Qiongdongnan Basin (in Chinese) [dissertation]. Wuhan: China University of Geosciences

van der Beek P, Van Melle J, Guillot S, et al. 2009. Eocene Tibetan plateau remnants preserved in the northwest Himalaya. Nature Geoscience, 2(5): 364–368, doi: 10.1038/ngeo503

van Hoang L, Wu Fuyuan, Clift P D, et al. 2009. Evaluating the evolution of the Red River system based on in situ U-Pb dating and Hf isotope analysis of zircons. Geochemistry, Geophysics, Geosystems, 10(11): Q11008

Wang Pinxian. 1995. ODP and Qinghai/Xizang (Tibetan) Palteau. Advance in Earth Sciences (in Chinese), 10(3): 254–257

Wang Guocan, Cao Kai, Zhang Kexin, et al. 2011a. Spatio-temporal framework of tectonic uplift stages of the Tibetan Plateau in Cenozoic. Science China Earth Sciences, 54(1): 29–44, doi: 10.1007/s11430-010-4110-0

Wang Xun, Liu Sheng'ao, Wang Zhengrong, et al. 2018. Zinc and strontium isotope evidence for climate cooling and constraints on the Frasnian-Famennian (~372 Ma) mass extinction. Palaeogeography, Palaeoclimatology, Palaeoecology, 498: 68–82

Wang Yingmin, Xu Qiang, Li Dong, et al. 2011b. Late Miocene Red River submarine fan, northwestern South China Sea. Chinese Science Bulletin, 56(14): 1488–1494, doi: 10.1007/s11434-011-4441-z

Wei Kuisheng, Cui Hanyun, Ye Shufen, et al. 2001. High-precision sequence stratigraphy in Qiongdongnan Basin. Earth Science-Journal of China University of Geosciences (in Chinese), 26(1): 59–66

Xie Xinong, Müller R D, Li Sitian, et al. 2006. Origin of anomalous subsidence along the northern South China Sea margin and its relationship to dynamic topography. Marine and Petroleum Geology, 23(7): 745–765, doi: 10.1016/j.marpetgeo.2006.03.004

Xiu Chun, Zhai Shikui, Huo Suxia, et al. 2018. Provenance of sediments of the Yacheng Formation in the Lingnan Low Uplift, Qiongdongnan Basin: Evidences from U-Pb dating of detrital zircons and geochemistry of the sediments. Bulletin of Mineralogy, Petrology and Geochemistry (in Chinese), 37(6): 1102–1113

Xu Qiang, Li Dong, Zhu Weilin, et al. 2020. Shrimp U-Pb ages of detrital zircons: Discussions on provenance control and the Red River capture event. Sedimentary Geology and Tethyan Geology (in Chinese), 40(3): 20–30

Xu Zhiqin, Yang Jingsui, Li Haibing, et al. 2011. On the tectonics of the India-Asia collision. Acta Geologica Sinica (in Chinese), 85(1): 1–33, doi: 10.1111/j.1755-6724.2011.00375.x

Yuan Shengqiang, Wu Shiguo, Yao Genshun. 2010. The controlling factors analysis of Qiongdongnan slope deepwater channels and its significance to the hydrocarbon exploration. Marine Geology and Quaternary Geology (in Chinese), 30(2): 61–66, doi: 10.3724/SP.J.1140.2010.02061

Zakharov Y D, Dril S I, Shigeta Y, et al. 2018. New aragonite $^{87}Sr/^{86}Sr$ records of Mesozoic ammonoids and approach to the problem of N, O, C and Sr isotope cycles in the evolution of the Earth. Sedimentary Geology, 364: 1–13, doi: 10.1016/j.sedgeo.2017.11.011

Zhong Dalai, Ding Lin. 1996. A discussion of the process and mechanism of Tibetan Plateau uplifting. Science in China Series D: Earth Sciences (in Chinese), 26(4): 289–295